Strain effect on the surface potential and nanoscale switching characteristics of multiferroic BiFeO3 thin films

F. Yan – Drexel University and National University of Singapore
S. Miao – Chinese Academy of Sciences
T. J. Zhu – Zhejiang University
M. O. Lai – National University of Singapore
L. Lu – National University of Singapore

Citation of published version:

Yan, F., Miao, S., Zhu, T., Lai, M., Lu, L. (2012): Strain effect on the surface potential and nanoscale switching characteristics of multiferroic BiFeO3 thin films. *Applied Physics Letters*, 100 (13). DOI: 10.1063/1.3698155

Strain effect on the surface potential and nanoscale switching characteristics of multiferroic $BiFeO_3$ thin films

F. Yan, S. Miao, T. J. Zhu, M. O. Lai, and L. Lu

Citation: Appl. Phys. Lett. **100**, 132907 (2012); doi: 10.1063/1.3698155
View online: https://doi.org/10.1063/1.3698155
View Table of Contents: http://aip.scitation.org/toc/apl/100/13
Published by the American Institute of Physics

Strain effect on the surface potential and nanoscale switching characteristics of multiferroic $BiFeO_3$ thin films

F. Yan,[1,4,a)] S. Miao,[2] T. J. Zhu,[3] M. O. Lai,[4] and L. Lu[4,b)]
[1]*Department of Materials Science and Engineering, Drexel University, Philadelphia, Pennsylvania 19104, USA*
[2]*Dalian Institute of Chemical Physics, Chinese Academy of Sciences, Dalian 116023, People's Republic of China*
[3]*Department of Materials Science and Engineering, Zhejiang University, Hangzhou 310027, People's Republic of China*
[4]*Department of Mechanical Engineering, National University of Singapore, Singapore 117576*

(Received 19 December 2011; accepted 10 March 2012; published online 28 March 2012)

The $BiFeO_3$ films were deposited on the $SrTiO_3$ (001) substrates via tuning the thickness of the $SrRuO_3$ (SRO) bottom electrode by pulsed laser deposition. The macroscopic ferroelectric and dielectric properties were dramatically impacted by the various nanoscale domain structures for both films due to the tunable SRO thickness. The nanoscale domain switching behaviors for both films were investigated via piezoresponse force microscopy, and results suggest that the domain structure could be changed by tuning the strain state. The surface potential investigation indicates that strain helps increase data storage density and stability. © *2012 American Institute of Physics*. [http://dx.doi.org/10.1063/1.3698155]

Lead-free $BiFeO_3$ (BFO) has received intensive study due to its rhombohedrally distorted perovskite structure at room temperature[1] with large polarization $\sim 100\,\mu C/cm^2$ along the (111) direction, high ferroelectric Curie temperature[2] ($T_C \sim 1123$ K), and antiferromagnetic Néel temperature[3] ($T_N \sim 647$ K). However, experimental results indicated that the epitaxial strain enhanced the spontaneous polarizations of BFO,[1] whereas calculations indicated that the magnitude of the polarization barely changed with changing strain, although the displacement mechanism can influence the stability of the ferroelectric state.[4,5] Meanwhile, experimental scenarios have been promoted to investigate the strain effects on polarization by fabricating the strain free membranes,[6] using substrates with different lattice parameters[7] ($DyScO_3$, $SrTiO_3$, $LaAlO_3$, etc), tuning the substrate miscut level,[8] and even forming a BFO nanostructured island.[9]

In this work, we change the strain state of BFO by tuning the bottom electrode thickness to obtain strain free polycrystalline and compressively epitaxial BFO films. The strain effect on the charge distribution and surface potential has been investigated, and its impacts on data storage properties have also been discussed. Furthermore, the strain dependent ferroelectric switching behaviors at macroscopic and microscopic scales have been investigated with a traditional ferroelectric tester and switching spectroscopy piezoresponse force microscopy (SS-PFM), respectively.

The BFO thin films (thickness of ~170 nm) with stoichiometric composition of $BiFeO_3$ were grown on (001)-oriented $SrTiO_3$ (STO) substrates using pulsed laser deposition (PLD), with a $SrRuO_3$ (SRO) layer serving as the bottom electrode. The growth temperatures of the SRO and BFO layers are 650 and 550 °C, respectively. The thickness of the SRO layer was 50 and 350 nm (indicated as thin and thick SRO, respectively), which was controlled via the deposition duration. Detailed deposition conditions of the thin films have been reported elsewhere.[10,11] The phase of the BFO films was characterized using x-ray diffraction with Cu $K\alpha$ radiation. Pt top electrodes (~100 μm in diameter) were sputtered on the surface to investigate the macroscopic electrical properties. The macroscopic ferroelectric and dielectric properties were recorded using a precision impedance analyzer with a vacuum MMR K20 temperature controller system and Radiant Precision Workstation, respectively. The surface topographies, surface potential, and local piezoresponse were examined using Asylum Research MFP-3D™ piezoresponse force microscopy (PFM), Kelvin probe force microscopy (KPFM), and the SS-PFM, respectively.

Figs. 1(a) and 1(e) show the x-ray diffraction θ-2θ patterns of the BFO films deposited on thick and thin SRO-buffered STO (001) substrates, respectively. The BFO with thin SRO reveals the epitaxial (00 l) ($l = 1, 2$) peaks without any impurity phases, whereas the BFO film with thick SRO presents a polycrystalline perovskite structure indexed as a pseudocubic unit cell. The values of pseudocubic lattice parameters are 4.047 and 3.961 Å for the BFO films with the thin and thick SRO layers, respectively. The corresponding misfit strains, compared with the bulk BFO (3.96 Å),[12] are −3.63% and −0.14%, respectively. This suggests that the BFO film with thick SRO exhibits strain relaxation properties, attributed to the thick SRO layer releasing the strain. Furthermore, the epitaxial arrangement of both films was studied using the pole figure measurement at a fixed 2θ scan of (101) reflection of the STO substrate, as shown in the insets of Figs. 1(a) and 1(e). The pole figures clearly indicate the "cube-on-cube" epitaxial growth of the BFO on the thin SRO layer, whereas the BFO on the thick SRO is relatively randomly oriented, indicating that the strain could greatly influence the growth behavior of the films.

a)Email: yf78@drexel.edu.
b)Email: luli@nus.edu.sg.

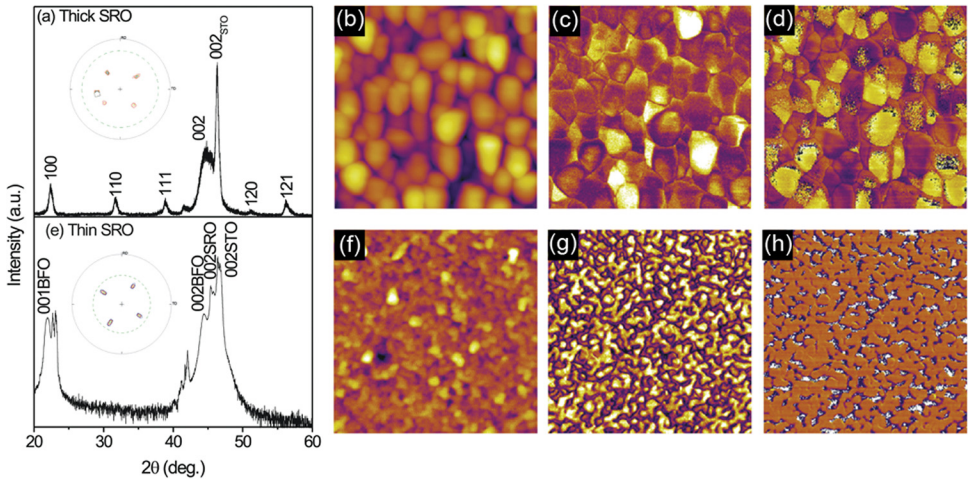

FIG. 1. (a), (e) XRD spectra of the BFO films with thick (350 nm) and thin (50 nm) SRO bottom electrode; the inset shows the pole figure of the BFO thin films on (101) plane. (b), (f) AFM images ($2 \times 2\ \mu m^2$); (c), (g) out-of-plane piezoresponse (OP-PFM) amplitude image; and (d), (h) OP-PFM phase image of BFO films. Yellow (bright) and purple (dark) on the PFM images correspond to upward and downward domains.

Figs. 1(b) and 1(f) show the surface morphologies of the BFO films with the thick and thin SRO layers, respectively. The root-mean-square (RMS) roughness obtained from the AFM measurements are 8.245 nm for the BFO with the thick SRO and 0.605 nm for that with the thin SRO, indicating that the roughness of the BFO film could be dramatically varied by changing the strain state of the films. Meanwhile, the resolved piezoresponse amplitude images of both BFO films, as shown in Figs. 1(c) and 1(g), reveal that most domains are limited by the grain boundaries in the BFO with the thick SRO, while that BFO with the thin SRO exhibits the mosaic domains with little correlation to topography as reported elsewhere.[13] Figs. 1(d) and 1(h) show the OP-PFM images. The ratios of the domains upward (bright yellow) and downward (dark purple) are 1:1 and 2:3 for the BFO films with the thin and thick SRO layer, respectively, indicating that the BFO with the thick SRO preferred downward polarization because the thicker bottom electrode caused more of a self-poling effect.[14]

Fig. 2(a) shows the ferroelectric polarization versus electric field (*P-E*) curves of both BFO films measured at 1 kHz at room temperature. The *P-E* loops show well-defined saturate shapes. The BFO with the thin SRO layer shows that the remanent polarization P_r is as high as 50 μC/cm^2, while that of the BFO with the thick SRO is 56 μC/cm^2. However, the saturated polarization $P_s \sim 61\ \mu C/cm^2$ and the coercive field $E_c \sim 520$ kV/cm are nearly the same for both BFO films. Fig. 2(b) shows the leakage current density J versus electric field E for both films. The BFO with the thin SRO exhibits a leakage current lower by nearly one order of magnitude compared with the BFO with the thick SRO. The decreased leakage current in the former can be due to the absence of conductive grain boundaries in the epitaxial film.

Fig. 2(c) illustrates the dielectric constant ε and dielectric loss $\tan\delta$ for both films as a function of frequency. The ε and $\tan\delta$ of the BFO with the thick SRO vary slightly from 80 to 70 and 0.013 to 0.025 with frequency, respectively, while the BFO with the thin SRO presents a much higher

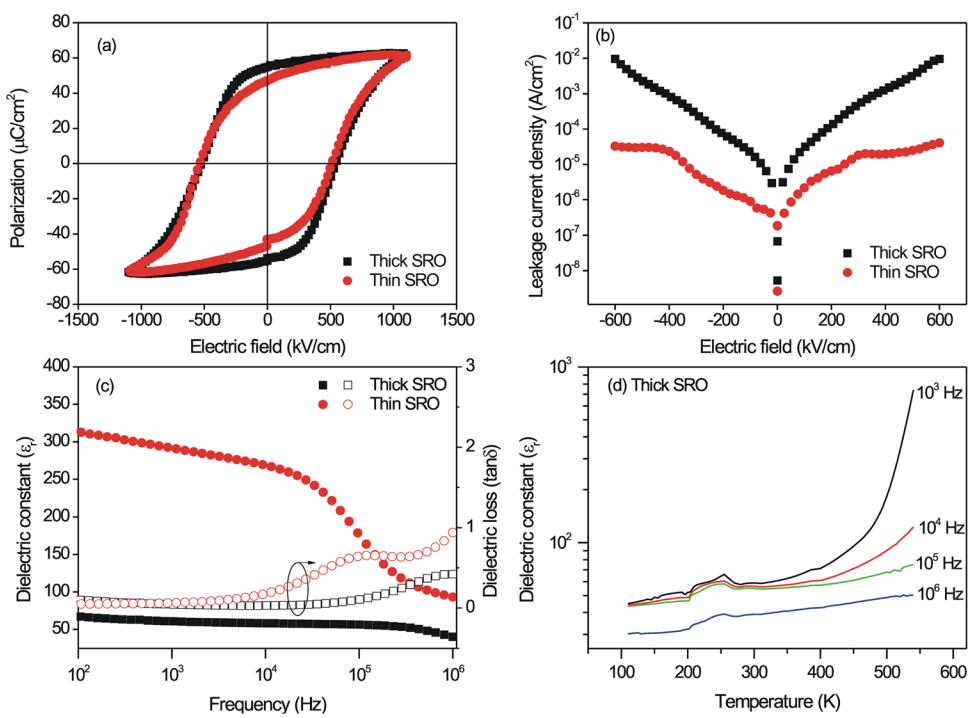

FIG. 2. (a) Polarization-electric field hysteresis (*P-E*) loops, (b) leakage current density (*J-E*), and dielectric properties as a function of (c) frequency and (d) temperature for BFO thin films with thin and thick SRO bottom electrodes.

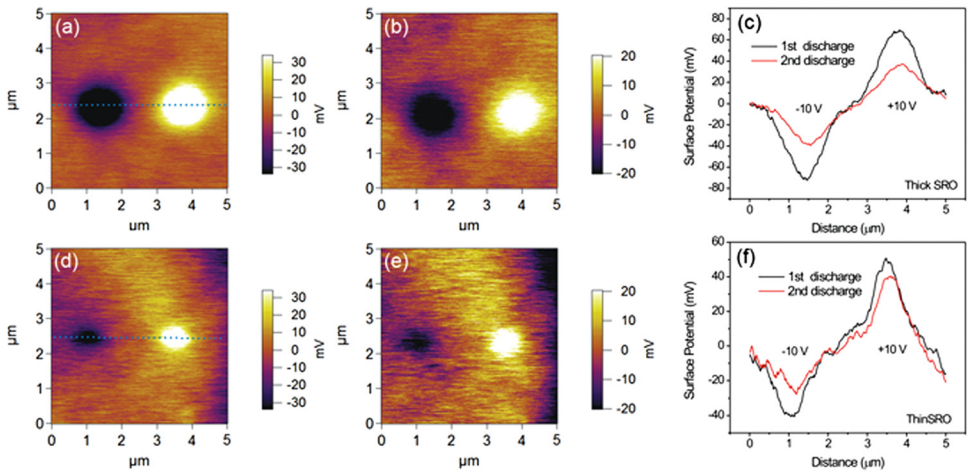

FIG. 3. (a), (d) Surface potential immediately, (b), (e) surface potential after second grounded tip scan (left: −10 V and right: +10 V); (c), (f) are their corresponding surface potential profiles under +10 and −10 V dc bias for BFO with thick and thin SRO, respectively (the profiles of surface potential are obtained according to the blue line indicated in (a) and (d).

$\varepsilon \sim 300$ at 1 kHz. By increasing the frequency up to 10^4 Hz, a sharp decrease of ε is correlated with a Maxwell-Wagner-type relaxation due to the space charges formed in the depletion interface between the BFO and SRO layers.[15] The greatly enhanced dielectric constant is due to the increased crystallinity and smaller roughness in the BFO film with the thin SRO layer.[16] At frequencies higher than 10^5 Hz, the increase in $\tan\delta$ implies that the charge carriers in the BFO with the thin SRO do not have time to respond to the external electric field[17] and a thicker SRO could largely suppress the electrical energy transferred to the oscillation ions.

Fig. 2(d) shows the frequency dispersion of the dielectric constant of the BFO with the thick SRO as a function of temperature at different frequencies. At temperatures below 300 K, two anomalies in the dielectric constant were observed at 200 and 250 K, which could be correlated with the spin reorientation transition at 200 K and spin glass behavior at 250 K. The spin frustration at 200 K for BFO comes from the phonon-magnon coupling.[18,19] At temperatures above 300 K, the ε shows a linear trend with temperature at a high frequency (1 MHz), presumably caused by the Maxwell-Wagner relaxation contribution to the dielectric constant, suggesting that a thicker SRO bottom electrode could maintain good temperature stability of the dielectric properties at high temperatures and frequencies.

In order to investigate the surface potential variation by a dc bias, the films were grounded and the tip was engaged onto the film surface for 1 min (writing process). Thus, the regions under the tip were injected by electrons or holes based on the applied tip voltage. Figs. 3(a) and 3(d) show the KPFM images obtained immediately after the poling process on the BFO with the thick and thin SRO bottom electrodes, respectively. The bright and dark dots present higher and lower surface potential values caused by dc bias at ±10 V, respectively, compared with the unpoled area. This suggests that both surface charges and ferroelectric polarization charges have been induced in the films. However, the BFO with the thick SRO shows a bigger dot size than that with the thin SRO, which can be attributed to the larger domain sizes in the BFO with the thick SRO. The corresponding surface charges increase as the poled area increases, indicating that the BFO with a thinner bottom electrode can possess a higher data storage density.

To further investigate the charge trapping and discharging properties, we performed a discharge process with a grounded tip (reading process) on the same area as mentioned previously.[20] The KPFM images, after the discharging process are shown in Figs. 3(b) and 3(e). Both positively and negatively poled areas become weakened for both films because the grounded tip swept partial surface charges and the polarization charges are dominant at the positively poled area.[21] Figs. 3(c) and 3(g) show the line profiles of the surface potential of Figs. 3(a) and 3(b) and Figs. 3(d) and 3(e), respectively. The surface potential decreases rapidly after

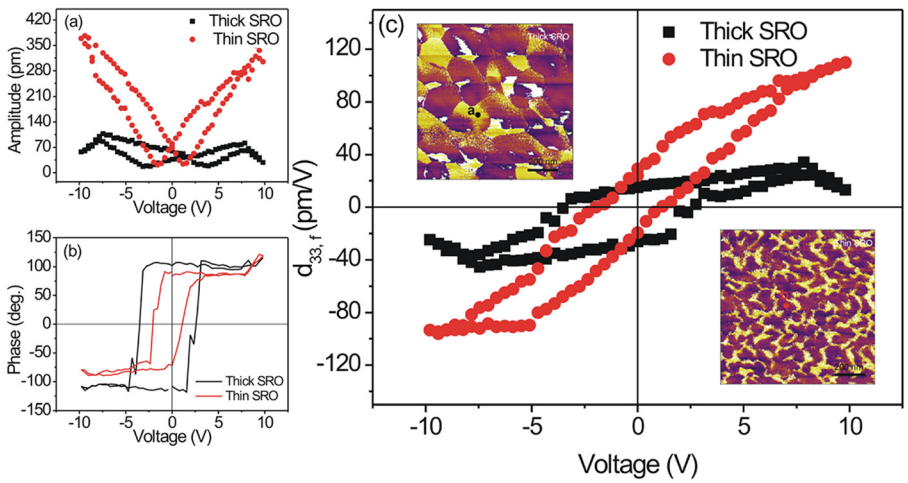

FIG. 4. Local piezoresponse (a) amplitude, (b) phase, and (c) effective $d_{33,f}$ hysteresis loops of BFO with thick and thin SRO measured at room temperature, respectively. The tip positions indicated by "a" and "b" are shown in the inset of (c), respectively.

the discharge process for the BFO with the thick SRO at both positively and negatively poled areas. This phenomenon indicates that the BFO with the thick SRO bottom electrodes can hold more surface charges and the trapped charges are injected deeply inside the film due to a high Schottky-type tunneling current.[20] However, the potential for the BFO with the thin SRO displayed a relatively slight decrease at the positively poled area, which is attributed to a small amount of overscreened charges[22] in this film. Therefore, the BFO with a thin bottom electrode can be more stable for data storage.

To ascertain the local switching behavior based on different strain states, microscopic ferroelectric switching properties were characterized for both films using the switching spectroscopy PFM (SS-PFM) technique.[23] Measurements performed at 10 V were repeated in 8 cycles to improve the signal-to-noise ratio.[24] Figs. 4(a) and 4(b) show the average SS-PFM amplitude (A) and phase (θ) loops for both BFO films. The loops of the amplitude and phase changes confirm a near complete polarization switching process.[25] Note that the switching process for the BFO with the thick SRO is partial with asymmetric amplitude loops, indicating the off-normal polarization direction and greater self-poling effects due to a thicker SRO layer,[14,25] in agreement with the macroscopic measurements. Meanwhile, the amplitude of the BFO with the thick SRO is lower than that of the BFO with the thin SRO, suggesting that the higher dielectric properties exist in the epitaxial film (Fig. 2(c)). Furthermore, the conceive field E_c (~200 kV/cm) observed from the local piezoresponse hysteresis loops is much smaller than that of the macroscopic P-E loops (520 kV/cm) because of the different switching mechanism between microscopic and macroscopic measurements.[23,26] Here, the E_c of the BFO with the thick SRO is larger than that of the BFO with the thin SRO as shown in the amplitude and phase loops, indicating that the domain switching in the polycrystalline film is more difficult than in the epitaxial film since there are a considerable number of domain wall pinning centers in the former.

The electromechanical response[27] of the surface was detected as $A = A_0 + A_{1\omega}\cos(\omega t + \varphi)$, where $A_{1\omega}$ is the amplitude of the first harmonic of the measured response and the effective piezoelectric coefficient[28] $d_{33,eff}$ can be roughly estimated as $d_{33,eff} = A_{1\omega}\cos\theta/V_{ac} = A\cos\theta$ as shown in Fig. 4(c), the tip positions also indicated in the insets of Fig. 4(c). The $d_{33,eff}$ hysteresis loops exhibit a slight offset, suggesting the presence of pinning centers between the tip-film interfaces during the domain growth.[23] The maximum and remanent $d_{33,eff}$ were determined to be 109.9 and 90.4 pm/V and 47.1 and 23.7 pm/V for the BFO with the thin and thick SRO, respectively. The enhanced $d_{33,eff}$ in the BFO with the thin SRO stems from the polarization vector being normal to the plane of the film, whereas the grains in the BFO with the thick SRO will have both in-plane and out-of-plane magnitudes for the piezoresponse.[29] Therefore, the piezoresponse would decrease in the off-axis orientation of the grains in polycrystalline films.[26] The BFO with the thin SRO displays markedly enhanced piezoelectric properties compared with that of the BFO with the thick SRO, but this result is in contrast to those obtained by studies of macroscopic ferroelectricity. The electrode based macroscopic ferroelectric hysteresis measurement ensures a uniform electric field in the film under the top electrode, whereas the SS-PFM technique appears to involve inhomogeneous electric/strain fields under the tips that are insufficient to produce a significant movement of domains at the nanoscale.[27] Hence, the SS-PFM hysteresis loops reveal the local ease of domain wall movement.

In summary, BFO films have been fabricated on the (001)-oriented STO substrates with different thickness of the bottom electrode in order to manipulate the strain state in the BFO. The film had a pure and polycrystalline phase at 350 nm SRO thickness while that with a 50-nm-thick SRO layer exhibited epitaxial growth behavior with ultra-smooth surface morphologies. The macroscopic ferroelectric and dielectric properties were dramatically impacted by the different nanoscale domain structures for both films due to the different SRO thicknesses. The domain structure and surface potential for both films have been investigated using the PFM and KPFM, indicating that the BFO with a thin bottom electrode could be helpful for data stability and high data storage density. Through local switching spectroscopy PFM investigations, the BFO with a thin bottom electrode displayed a higher piezoresponse constant compared with that of the BFO with a thick electrode.

[1] J. Wang, J. B. Neaton, H. Zheng, V. Nagarajan, S. B. Ogale, B. Liu, D. Viehland, V. Vaithyanathan, D. G. Schlom, U. V. Waghmare, N. A. Spaldin, K. M. Rabe, M. Wuttig, and R. Ramesh, Science **299**, 1719 (2003).
[2] J. B. Neaton, C. Ederer, U. V. Waghmare, N. A. Spaldin, and K. M. Rabe, Phys. Rev. B **71**, 014113 (2005).
[3] C. Ederer and N. A. Spaldin, Phys. Rev. B **71**, 060401(R) (2005).
[4] H. Ma, L. Chen, J. Wang, J. Ma, and F. Boey, Appl. Phys. Lett. **92**, 182902 (2008).
[5] C. Ederer and N. A. Spaldin, Phys. Rev. Lett. **95**, 257601 (2005).
[6] H. W. Jang, S. H. Baek, D. Ortiz, C. M. Folkman, R. R. Das, Y. H. Chu, P. Shafer, J. X. Zhang, S. Choudhury, V. Vaithyanathan, Y. B. Chen, D. A. Felker, M. D. Biegalski, M. S. Rzchowski, X. Q. Pan, D. G. Schlom, L. Q. Chen, R. Ramesh, and C. B. Eom, Phys. Rev. Lett. **101**, 107602 (2008).
[7] R. J. Zeches, M. D. Rossell, J. X. Zhang, A. J. Hatt, Q. He, C.-H. Yang, A. Kumar, C. H. Wang, A. Melville, C. Adamo, G. Sheng, Y.-H. Chu, J. F. Ihlefeld, R. Erni, C. Ederer, V. Gopalan, L. Q. Chen, D. G. Schlom, N. A. Spaldin, L. W. Martin, and R. Ramesh, Science **326**, 977 (2009).
[8] J. W. Park, S. H. Baek, P. Wu, B. Winchester, C. T. Nelson, X. Q. Pan, L. Q. Chen, T. Tybell, and C. B. Eom, Appl. Phys. Lett. **97**, 212904 (2010).
[9] S. H. Baek, H. W. Jang, C. M. Folkman, Y. L. Li, B. Winchester, J. X. Zhang, Q. He, Y. H. Chu, C. T. Nelson, M. S. Rzchowski, X. Q. Pan, R. Ramesh, L. Q. Chen, and C. B. Eom, Nat. Mater. **9**, 309 (2010).
[10] F. Yan, T. J. Zhu, M. O. Lai, and L. Lu, Scr. Mater. **63**, 780 (2010).
[11] F. Yan, M.-O. Lai, L. Lu, and T.-J. Zhu, J. Phys. Chem. C **114**, 6994 (2010).
[12] S. Y. Yang, F. Zavaliche, L. Mohaddes-Ardabili, V. Vaithyanathan, D. G. Schlom, Y. J. Lee, Y. H. Chu, M. P. Cruz, Q. Zhan, T. Zhao, and R. Ramesh, Appl. Phys. Lett. **87**, 102903 (2005).
[13] G. Catalan, H. Béa, S. Fusil, M. Bibes, P. Paruch, A. Barthélémy, and J. F. Scott, Phys. Rev. Lett. **100**, 027602 (2008).
[14] Y. H. Chu, T. Zhao, M. P. Cruz, Q. Zhan, P. L. Yang, L. W. Martin, M. Huijben, C. H. Yang, F. Zavaliche, H. Zheng, and R. Ramesh, Appl. Phys. Lett. **90**, 252906 (2007).
[15] M. Y. Seyidov, R. A. Suleymanov, Y. Bakis, and F. Salehli, J. Appl. Phys. **108**, 074114 (2010).
[16] S. H. Lim, M. Murakami, J. H. Yang, S. Y. Young, J. Hattrick-Simpers, M. Wuttig, L. G. Salamanca-Riba, and I. Takeuchi, Appl. Phys. Lett. **92**, 012918 (2008).
[17] J. Chen, X. Xing, A. Watson, W. Wang, R. Yu, J. Deng, L. Yan, C. Sun, and X. Chen, Chem. Mater. **19**, 3598 (2007).
[18] K. S. Manoj, R. S. Katiyar, and J. F. Scott, J. Phys.: Condens. Matter **20**, 252203 (2008).
[19] J. F. Scott, M. K. Singh, and R. S. Katiyar, J. Phys.: Condens. Matter **20**, 322203 (2008).

[20]Q. Zhang, C. H. Kim, Y. H. Jang, H. J. Hwang, and J. H. Cho, Appl. Phys. Lett. **96**, 152901 (2010).
[21]J. Son, B. Kim, C. Kim, and J. Cho, Appl. Phys. Lett. **84**, 4971 (2004).
[22]Y. Kim, C. Bae, K. Ryu, H. Ko, Y. K. Kim, S. Hong, and H. Shin, Appl. Phys. Lett. **94**, 032907 (2009).
[23]S. Jesse, A. P. Baddorf, and S. V. Kalinin, Appl. Phys. Lett. **88**, 062908 (2006).
[24]S. Jesse, H. N. Lee, and S. V. Kalinin, Rev. Sci. Instrum. **77**, 073702 (2006).
[25]D. Mazumdar, V. Shelke, M. Iliev, S. Jesse, A. Kumar, S. V. Kalinin, A. P. Baddorf, and A. Gupta, Nano Lett. **10**, 2555 (2010).
[26]S. Kalinin, A. Gruverman, and D. Bonnell, Appl. Phys. Lett. **85**, 795 (2004).
[27]Z. Tan, A. L. Roytburd, I. Levin, K. Seal, B. J. Rodriguez, S. Jesse, S. Kalinin, and A. Baddorf, Appl. Phys. Lett. **93**, 074101 (2008).
[28]D. Y. Wang, N. Y. Chan, S. Li, S. H. Choy, H. Y. Tian, and H. L. Chan, Appl. Phys. Lett. **97**, 212901 (2010).
[29]S. Wicks, V. Anbusathiah, and V. Nagarajan, Nanotechnology **18**, 465502 (2007).